Name of participating team member: Kuang Cheng Yu, Li Fu Zhi

School Name: Dulwich International High School Zhuhai

Province / State: Guangdong, Zhuhai

Country / region: China

Name of instructor: Nandish Shah

Essay topic: Ferrous Ion Immobilized Carbon Dots Fluorescent Sensing Platform for Homogeneous Glucose Detection based on Fenton Reaction

The participating team declares that the papers submitted are research work and research results obtained under the guidance of the instructor. To the best of the team's knowledge, the paper does not contain research results that have been published or written by other people, except for the content listed in the text and the acknowledgment. If there is any inaccuracy, I am willing to bear all related responsibilities.

Participants: Kuang Cheng Yu，Li Fu Zhi **Instructor:** Nandish Shah

Date: 20200910

Kuang Cheng Yu, Li Fu Zhi

Abstract:

In this study, we proposed a facile synthesis, low cost, and environmentally friendly glucose detection system. The methodology employed is measuring the fluorescence intensity of a developed Fe (II) carbon quantum dot complex (Fe (II)-CDs) to assess glucose level, where the fluorescence of Fe (II)-CDs is quenched by the production of hydroxyl radicals via Fenton reaction between Fe (II) and H_2O_2, which is produced by the reaction between glucose and glucose oxidase. Hydrothermal treatment is employed for carbon dot manufacture using citric acid and urea as precursors. TEM, XPS, FTIR and zeta potentials are measured to characterize the as-prepared Fe (II)-CDs. Hydroxyl radicals destruct Fe (II)-CDs' structure is supposed to be the quenching mechanism. The developed glucose detection system was analyzed with H_2O_2 and glucose respectively. A linear range (0.005 to 1.25 mM) and a detection limit (1.42 μM) for glucose detection is obtained. The analyzation of glucose level in serum sample demonstrated the developed system's potential in diabetes diagnose.

Key words:

Carbon dot, fluorescence, oxidative quenching, glucose detection, diabetes diagnoses

Table of Contents:

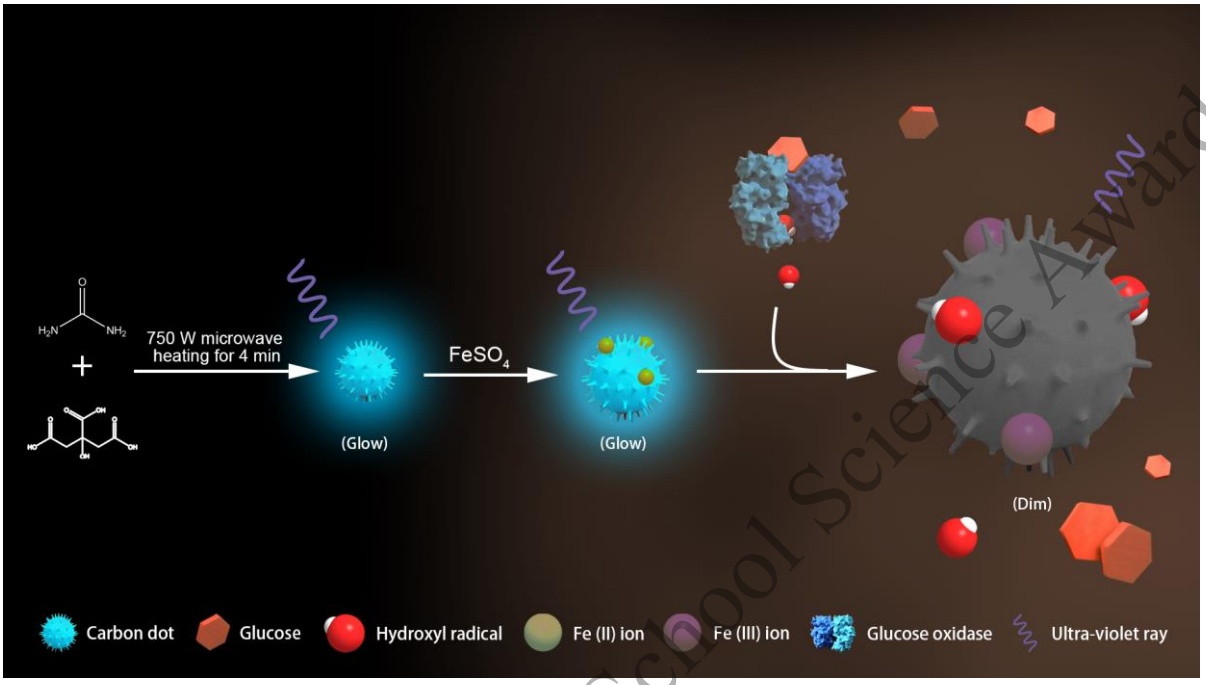

Contents

1. Introduction

Millions of people in the world is diagnosed with diabetes. A WHO study claims that there are 300 million diabetes diagnosed patients in 2013, and they are expecting this number to be doubled by 2030 [1]. The disease is caused by insulin deficiency and therefore patient's blood glucose level is usually high [2]. Diabetes often accompanied by fearful late complications like blindness, visual impairment, renal failure, stroke, and amputation [3][4]. Therefore, it is vital to diabetes patients' life quality to design and develop an effective and efficient analytical strategy. Clinical diagnosis of diabetes requires frequently monitoring the patient's plasma glucose level [4][5]. For this reason, the determination of the concentration of blood glucose with selectivity and sensitivity is of great importance. A healthy individual's blood glucose level is between 3.9-6.1 mM in whole blood and between 3.9-6.9 mM in plasma, whereas for a diabetes diagnosed patients, their whole blood glucose level is more than 6.1 mM or 7 mM in plasma [6]. Due to the complicated blood composition [7], it is necessary to dilute blood plasma before glucose detection. Considering the relatively low percentage glucose takes in blood, it is necessary for a sensitive glucose detection system to be developed.

Recently, numerous efforts have been made to detect blood glucose levels and various techniques has been utilized, which includes but not limited to electrochemistry [8], mass spectrometry [9], surface-enhanced Raman scattering [10], colorimetry [11], chemiluminescence [12], and fluorescence [13]. Particularly, fluorescent nanomaterials demonstrate great potential in sensing applications as they own a high level of sensitivity and simple modification characteristics.

Carbon quantum dot (CDs), usually referred to carbon dots, is a kind of label-free fluorescence nanomaterial that researchers have shown great interest in. It has been considered as a potential candidate for sensing, drug delivery and imaging applications. In comparison with other quantum dots, such as semiconductor quantum dots, CDs stands out owing to its' biocompatibility, the ability to form a homogeneous solution, and plentiful edge sites for functionalization [14].

Herein a kind of CDs with a high quantum yield (QY) of 18.87% is developed with characteristics of low cost, nontoxic, and label-free. A glucose detection system is designed utilizing the developed CD. The detection process involves mixing serum sample and CDs and

glucose level is detected by measuring CDs' fluorescence intensity. Series of chemical reactions take place within the detection system: First, H_2O_2 is produced by the reaction between glucose and glucose oxidase (GOx). Then, Fe (II) and H_2O_2 react to produce hydroxyl radicals via Fenton reaction. Finally, destructions on CDs structure is caused by hydroxyl radicals, which cause fluorescence quenching.

One of the advantages of the developed system is that environmentally friendly chemicals – urea and citric acids – are employed as precursors. Either of them has become one of the common recipes used in food, pharmaceuticals, cosmetic, and dietary supplements. For this reason, this type of fluorescent material is suitable for biologically related researches. In light of the above-mentioned reasons, the developed glucose detection system has potential in further developments in detection applications, in this case, glucose measurement in human serum sample.

2. Experimental

2.1 Instrumentation

Table 1 Instrumentation

Instrument	Type	Manufacturer
FT-IR spectrometer	PE Spectrum One	PE, USA
Electron spectrometer	Thermo ESCALAB 250XI	Thermo, USA
Transmission electron microscope	Tecnai G2 F30	FEI, USA
Fluorescence Spectrophotometer	F-7000	Hitachi, Japan
Spectrophotometer	U-3900	Hitachi, Japan
Zetasizer	ZS 90	Malvern panalytical, UK
Fluorescence Spectrometer	FLS980	Edinburgh Instruments Ltd., UK

2.2 Materials

Table 2 Materials (All chemicals were analytical reagent grade.)

Materials	Manufacturer
IFN-γ	Sigma
Thrombin	Sigma
Lactose	Sigma
PDGF-BB	Sigma
Urea	Sigma
Citric acid	Sigma
Fluorescence Spectrometer	Sigma
Glucose	Sangon Biotech Co. Ltd.
BSA	Sangon Biotech Co. Ltd.
Glucose oxidase	Sangon Biotech Co. Ltd.
H_2O_2 (20%)	Sinopharm Chemical Reagent Co., Ltd.
$FeSO_4 \cdot 7H_2O$	Xilong Chemistry Co. Ltd.
NaCl	Xilong Chemistry Co. Ltd.
$CaCl_2$	Xilong Chemistry Co. Ltd.
$MgCl_2 \cdot 6H_2O$	Xilong Chemistry Co. Ltd.
$FeCl_3$	Xilong Chemistry Co. Ltd.
KCl	Xilong Chemistry Co. Ltd.
NaOH	Xilong Chemistry Co. Ltd.

2.3 Experimentation

2.3.1 Preparation of CDs

A domestic microwave oven with 750 W is employed for heating the a solution - which was consisted of 1.5 g citric acid, 3.0 g urea and 20 mL water - for approximately 4 minutes (with no cover to prevent water evaporation). The initial colorless solution then darkened its color and eventually solidified into a dark solid. After that, the solid - which is the CDs formed - was re-dissolved using ultra-pure water. It was then filtered (0.22-μm pore diameter) to remove aggregated particles. Further purification was done by dialysis in water using a membrane (MWCO = 1000 KD Shanghai Yuanye Biological Technology Co., Ltd.). After that, a transparent, light-yellow CDs solution was obtained. It is then freeze dried for further use.

2.3.2 Synthesis of Fe (II)-CDs

Fe (II)-CDs was prepared by simply mixing $FeSO_4$ (0.5 mM) aqueous solution and 2.5 mg/mL CDs suspension together, which is then stirred for 40 minutes in room-temperature. After that, the product produced was dialyzed in deionized water for 4 h.

2.3.3 H_2O_2 detection

H_2O_2 detection has been done in a 100 μL mixture, which contains 20 μL H_2O_2 with different concentrations, 10 mM PBS (pH 6.0), and 10 μL 1.4 mg/mL Fe (II)-CDs. An incubation was performed for the mixture at 37℃ for 20 minutes. After that, a fluorescence spectrum was then recorded on F-7000 fluorescence spectrophotometer.

2.3.4 Pretreatment for human serum

We took human serum sample from the local hospital. 250 L human whole blood samples were taken and centrifuged in a 1.5 mL centrifuge tube (1.2×10^4 r/min at 4 ℃ for 20 min). Then a refrigerator is used for storing the supernatant at 4 ℃ for later use.

2.3.5 Glucose detection

Glucose detection was operated as the following: mixtures consist of 5 μL GOx (3.0 mg/mL), 35 μL of PBS solution (10 mM, pH 6.0), and 20 μL of glucose solution with different concentrations were prepared. They were then added into a 0.6 mL centrifuge respectively. The product was incubated at a temperature of 37 ℃ for 25 minutes. Finally, 10 μL of Fe (II)-CDs with a concentration of 1.4 mg/mL and 30 μL of PBS solution with a concentration of 10 mM,

pH 6.0 was added into the solution. After well mixed the solution, the fluorescence spectra were recorded.

3. Result and discussion

3.1 Characterization of CDs and Fe (II)-CDs

The as-prepared CDs' and Fe (II)-CDs' exterior were observed. An image was taken with the use of transmission electron microscopy (TEM) for CDs and Fe (II)-CDs (figure 1a and 1b), which show that both CDs and Fe (II)-CDs are uniformly distributed in the solution, indicating they have the potential to form a homogeneous mixture in serum sample. The distance between each CDs and Fe (II)-CDs in the solution is approximately 4-5 nm. The inserted images in both figure 1a and 1b are their own HRTEM respectively. They demonstrate that in each ball-like structure, there are evenly distributed crystal lattices inside. The distance between each lattice is 0.33 nm in average. Owing to the similar fluctuation in diameter, the size distribution of both CDs and Fe (II)-CDs are both illustrated in figure 1c. It can be inferred that the diameters fluctuate in the range of 2.50-4.00 nm, and the majority of them concentrated in the range of 3.25-3.75 nm.

The CDs' and Fe (II)-CDs' spectral characteristics are recorded, which includes Fourier transform infrared spectroscopy (FTIR), X-ray photoelectron spectroscopy (XPS), and ultraviolet–visible spectroscopy (UV-vis).

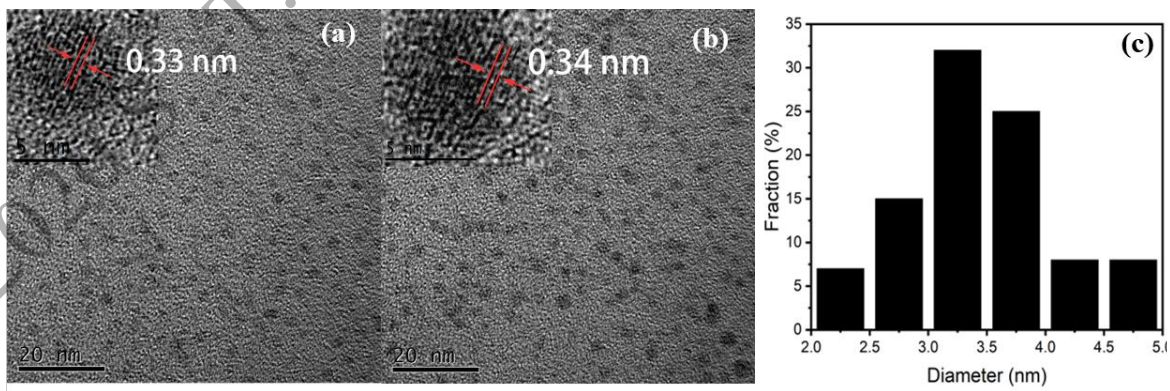

Figure. 1 TEM, HRTEM (inset) image of the CDs (a), Fe (II)-CDs (b). The diameter distribution of CDs and Fe (II)-CDs (c).

The full-scan XPS spectrum (figure 2a) exhibits three peaks at 284.97, 389.97, and 530.97 eV, which represent C 1s, N 1s, and O 1s respectively. Figure 2b is the full-scan XPS spectrum of Fe-doped CD where three major peaks at 283.97, 398.97, 530.97 eV pointed out the existence of C 1s, N 1s, O 1s. In addition, an element ratio is analyzed for CDs is 53:23:24 (C:N:O) and for Fe (II)-CD is 54:17:26:3 (C:N:O:Fe). Furthermore, figure 2c, which is an enlarged segment of figure 2b, has two peaks at 711.17 and 725.12 eV, which proved the ferric ion on CDs is Fe (II). Meanwhile, the HRXPS spectra of CD's C 1s (figure 2d) can be well assigned into four surface components: C-C (sp2)'s binding energy at 284.62 eV, C-C (sp) at 285.22 eV, C-O at 286.62 eV and C=O at 288.57 eV. Considering carboxyl group and hydroxyl group are in included in citric acids and amino group is included in urea, it is supposed that phenolic hydroxyl group (hydroxyl groups), amino groups, and carboxyl groups exists on the CDs and Fe (II)-CDs. In addition, the well dissipative in water of CDs and Fe (II)-CDs can attribute to the presence of hydroxyl groups.

FTIR spectra were recorded at room temperature for both CD and Fe (II)-CD complex (figure 3a). For Fe (II)-CD complex, the broad peaks at 698, 2079 and 3402 cm^{-1} ascribed to C-H, R-

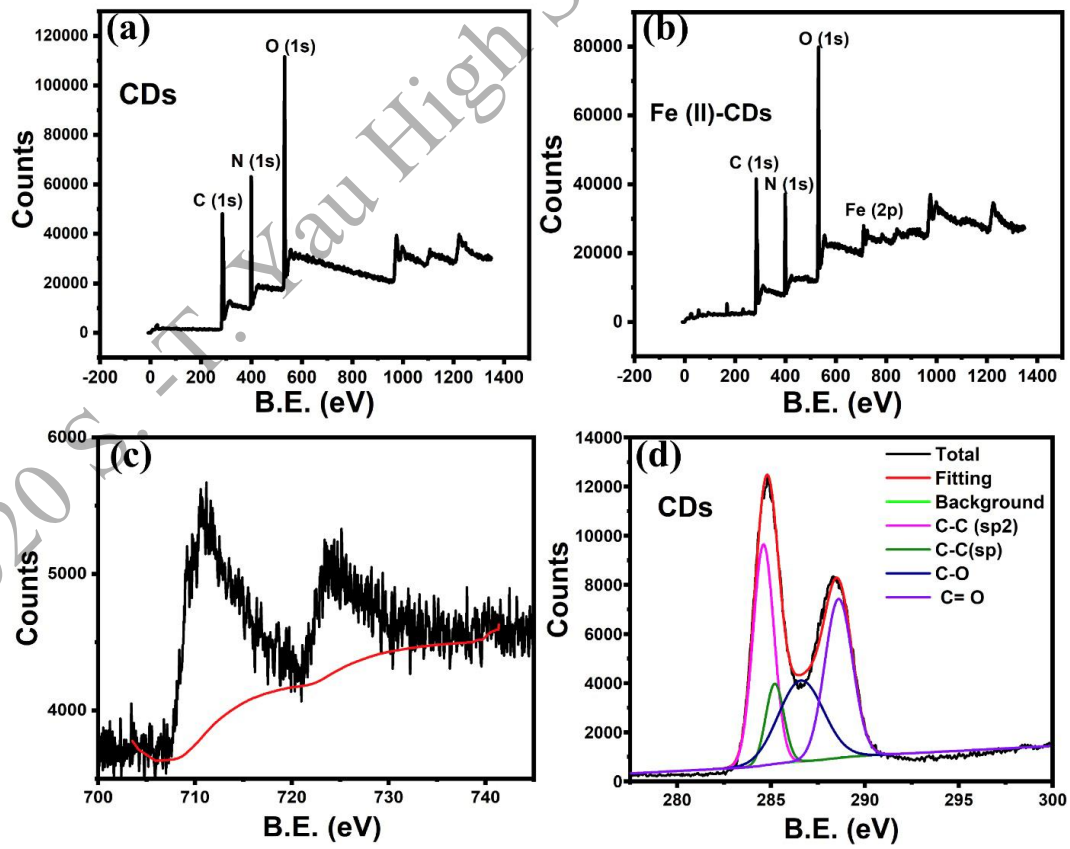

Figure. 2 The XPS survey spectrum of CDs (a), Fe (II)-CDs (b), and Fe 2p XPS spectrum (c), C 1s XPS spectrum of the as-prepared Fe (II)-CDs (d).

C=C-H, and O-H / N-H stretching vibration respectively, whereas the other two peaks at 1639 and 2374 cm^{-1} can be assigned to C-O and O=C=O stretching. Similarly, for CD, the stretching frequencies at 692, 1639, 2086, 2376, and 3429 cm^{-1} indicates the existence of C-H, C=O, R-C=C-H, O=C=O, and O-H / N-H bonds. The above-mentioned analytical results further confirmed the existence of amino groups, carboxyl groups and phenolic hydroxyl group (hydroxyl groups) on both CDs and Fe (II)-CD complex.

3.2 Optical properties of CDs and Fe (II)-CDs

The as-prepared CDs' and Fe (II)-CDs' UV-vis absorption spectrums are obtained (figure 3b), which displayed two shared absorption peaks (one on 220 nm and another one on 345 nm), and these peaks may represent the p-π* and n-π*electron orbital transition that correlates to C=C bond [15] and C=O bond [16] respectively.

The emission spectrum of as-prepared CDs is shown in figure 3c. Despite that there are some variations in terms of the emission intensity, the wavelength of fluorescence emission peak does not change with the adjustment of the wavelength of the inducing ultra-violet light. An ultra-violet ray with wavelength of 360 nm can induce the highest fluorescence intensity at around 445 nm, which can be viewed as a blue light (inset of figure 3c). This shows a broad stokes shift of 85 nm [17]. Additionally, the as-prepared CDs also demonstrate an excitation-dependent behavior: the intensity of the emission spectrum decreases with the red-shift (lower energy emission) of the excitation UV wavelength. The quantum yield (QY) is measured, and the result calculated was 18.87 %, which is competitive among other CDs made through similar hydrothermal methods [18-22].

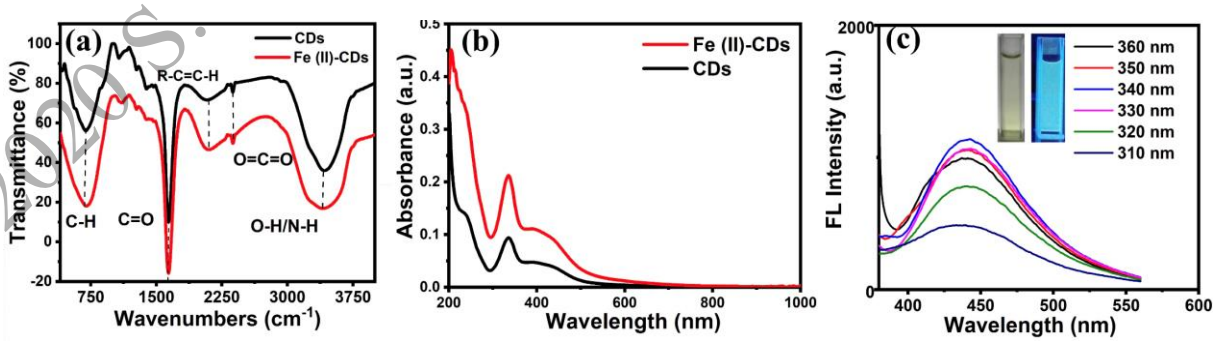

Figure. 3 FTIR spectra (a), UV/Vis absorption spectrum (b), and the luminescent of Fe (II)-CDs at excitation wavelength within the range of 310-360 nm, the inset within is the photo of CDs (the one in visible light and the one under UV light) (c).

3.3 As-prepared CD's stability test

For the sake of the examination on the feasibility of the as-prepared CDs in terms of its glucose detection applications, the as-prepared CDs' photostability is analyzed. The CDs' fluorescence intensity is obtained in solutions of different pH levels and NaCl concentrations. Figure 4a demonstrated that the CDs' fluorescence intensity fluctuates little in different pH environment ranging between 4-8 pH. This shows the relatively high resistance to protonation and deprotonation to the surrounding of the as-prepared CDs [23]. In consider of the large amounts of sodium element existing in the human serum, it is vital for CDs to remain stable in NaCl solutions with different concentrations [8]. Figure 4b illustrates that the fluorescence intensity of CDs fluctuates around 750 a.u. with a variety of NaCl concentrations ranging between 0-2 mM, which displays the as-prepared CDs' relatively high photostability in NaCl solution [24]. In light of these two results, we believe that the as-developed glucose detection system possesses the potential to be applied on human serum glucose level detection.

3.4 Fluorescence mechanism

The mechanism for blue fluorescence is explained in the following section. The fluorescence mechanism of CDs is similar to that of the UV-vis spectroscopy. To illustrate, as demonstrated in figure 5, the photon that is fertilized by the ultra-violet emitter hit the surface of the CDs and induced a series of electron transitions. The energy that the photon carries can transfer to the electron that can be found in either p or δ orbitals as long as it exceeds the energy in the energy

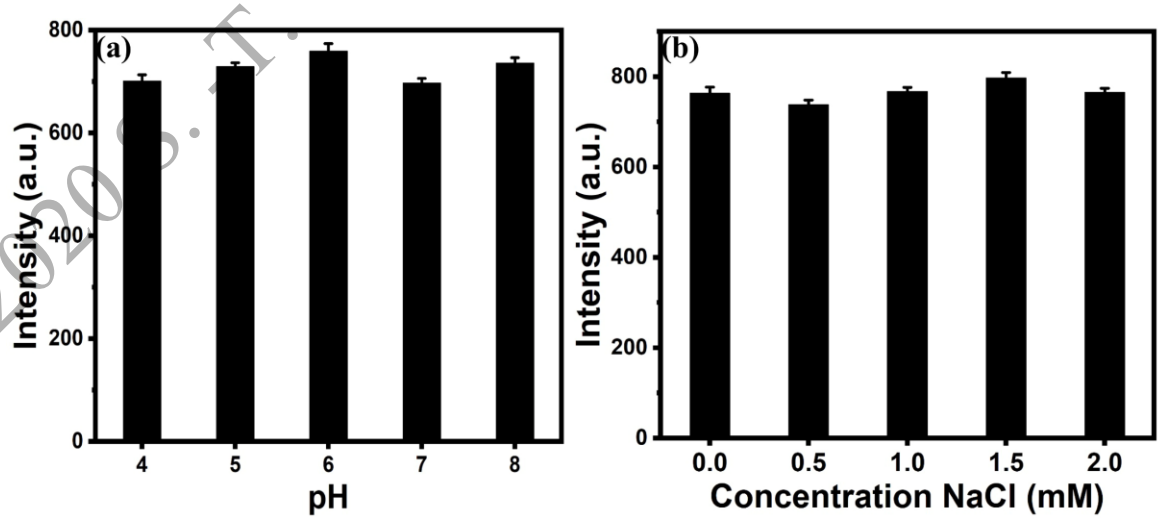

Figure 4 The CDs' fluorescence intensity in 5 distinct pH environment (a). The CDs fluorescence intensity in 5 distinct NaCl concentrations ranging from 0-2 mM (b).

band gap between that electron's exited state and it ground state. The electrons which stays on their highest occupied molecular orbital (HOMO) may be excited and transfer to their lowest unoccupied molecular orbital (LUMO). While the electron is returning from its LUMO to its HOMO, there can be the emission of electromagnetic radiation, and some may be emitted as visible light. Besides, since the π to π* bond transfer on the carbide core and the n to π* bond transfer on the functional groups is considered as the CDs' crucial fluorescence sources. Therefore, the structure of the carbide core and functional group on CDs' surface is vital to CDs' properties, especially that of optical [25]. To demonstrate, the increase in terms of the size of CDs' core will lead to the red-shift of emission because the increased level of sp2 hybridized orbital will decrease the bandgap of the CDs [26]. The size of our CDs is mainly in the range of 3.25-3.75 nm (figure 1c), which belongs in the visual light emission range [25]. In addition, a higher surface oxidation level may also cause a red-shift emission. This is because the electron may shift into a lower energy emissive site first with no electromagnetic radiation emission [27]. Then, when the electron transferred onto its HOMO, there can be fluorescence. For this reason, the wavelength of the fluorescence of the oxidized CDs becomes higher in comparison with that of the normal CDs as the bandgap for fluorescence is smaller [28]. It is possible for CDs to emit electromagnetic radiation that has a low wavelength and high frequency, which can be out of the visible range. According to the XPS and FTIR spectrum, which demonstrates the high level of oxidation of our as-prepared CDs, it is reasonable to infer that the as-prepared CDs may emit visible light, for example, having a blue emission peak.

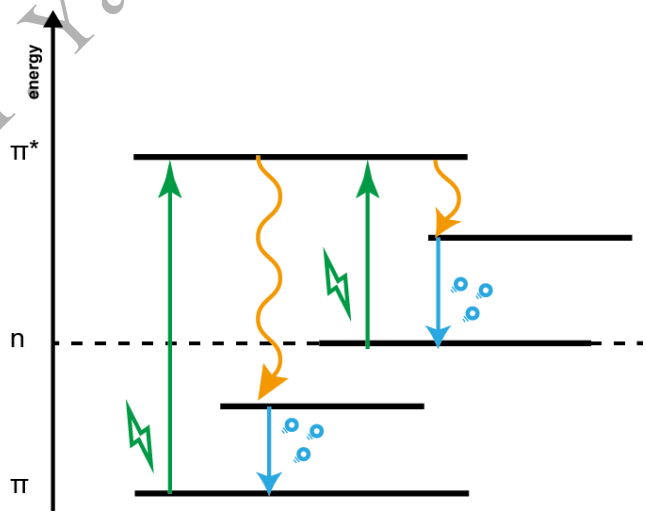

Figure 5 CDs fluorescence mechanism

3.5 Fluorescence quenching mechanism

This section will first discuss several possible quenching mechanisms that we supposed existence in our experiment: Inner Filter Effect (IFE), Photoinduced Electron Transfer (PET) and Oxidative Quenching (OQ). Then, it will be demonstrated why it is supposed that OQ plays the most role.

Figure 6a provided supports in terms of speculating potential quenching mechanisms as it lists possible chemical combination scenarios that can occur during our experiment. We can infer that among various chemical combinations, the groups for Fe (II)-CDs and H_2O_2 stands out as this group displays the lowest fluorescence intensity.

Numerous assays have reported different metal ions' quenching ability on CDs. It is worth noting that Fe (III) is the best fluorescence quenching candidate as it displays outstanding

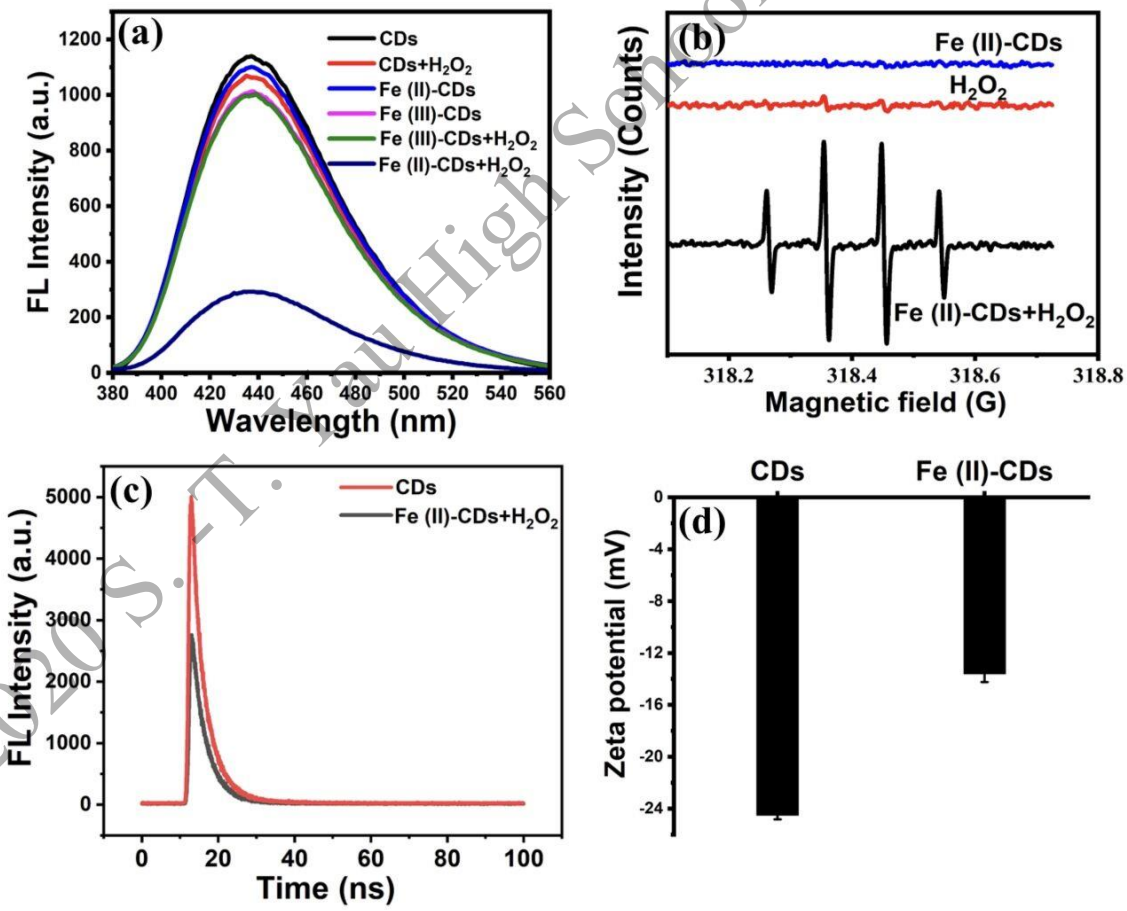

Figure. 6 The fluorescence spectrum of CDs, Fe (II)-CDs, Fe (III)-CDs, Fe (II)-CDs + H_2O_2, Fe (III)-CDs+H_2O_2 system (a). The ESR spectroscopy of Fe (II)-CDs, H_2O_2, and Fe (II)-CDs + H_2O_2 (b). The fluorescence life time of CDs and Fe (II)-CDs + H_2O_2 (c). Zeta potential measurement of CDs and Fe (II)-CDs (d).

quenching ability [29-31]. Therefore, it is reasonable to conclude that ferric ion is a possible quencher for the as-prepared CDs. Owing to the existence of Fenton reaction, which is proved existence by figure 6b [29][30], it is assumed Fe (III) ions, hydroxyl radicals, and hydroxide ions exist in our experiment.

Since in figure 6c the fluorescence lifetime of as-prepared CDs has no obvious change either when Fe (II) is present or absent, dynamic (collisional) quenching have a bigger impact [32][33]. The ultra-violet absorption spectrum (figure 3b) also supports this view because there is no apparent variation between CDs and Fe (II)-CDs absorbance signal [33]. It is well known that Fe (III) ion trends form a complex with amino, carboxyl, and hydroxyl (phenolic hydroxyl) groups, which is considered to promote charge transfer, restrain excited electron and therefore leading to fluorescence quenching [34-36]. Figure 6d indicates that Fe (II)-CDs has a higher zeta potential, which represents a complex is formed between the functional groups that possess negative charges and the Fe (II) ions that has positive charges. For this reason, it is supposed that one of the factors contributing to the as-prepared CD's fluorescence quenching is PET, for there is a complex exists between the quencher and the fluorophore [32]. However, Figure 6a implies the as-prepared CD has slightly quenched by iron ions and therefore PET should not have a big impact on CD fluorescence quenching.

Furthermore, the absorption spectrum of hydroxyl radicals is in the 200-300 nm region whereas that of the as-prepared CDs is approximately in it 294-386 nm region (figure 3b) [37]. Moreover, the absorption spectrum of hydrogen peroxide is 210-350 nm [38]. For this reason, the three overlapping spectrums are the evidences for the occurrence of the IFE that contribute to the fluorescence quenching of the as-prepared CD [39]. However, H_2O_2 and hydroxyl radicals may only exert a negligible effect and it should not be a dominant fluorescence quenching factor. According to the Fenton reaction, Fe (II) reacts with H_2O_2 to produce hydroxyl radicals which have ultrahigh oxidation potential. It is supposed that reactions will happen between the oxidative hydroxyl radicals and the reductive functional groups, which composed CDs' surface structure. This can lead to changes in the structure of the CDs [40][41]. It is mentioned before that CDs' structure is crucial to its fluorescence ability, the damage caused by hydroxyl radicals on surface functional groups causes the intense level of fluorescence quenching illustrates in figure 6a.

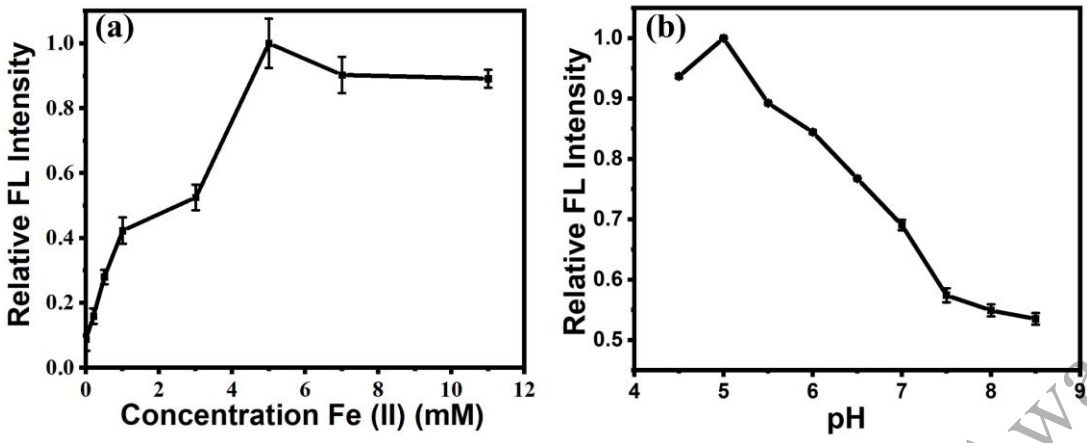

Figure. 7 The variations of Fe (II)-CDs' fluorescence intensity with different addition of Fe (II) (a). The fluctuations of Fe (II)-CDs' fluorescence intensity with 6 distinct pH levels (b).

3.6 Glucose detection system

As mentioned before, the developed glucose detection methodology can be split into three steps. First, glucose oxidase (GOx) oxidize glucose and produce H_2O_2. After that, the H_2O_2 produced reacts with Fe (II) and produce hydroxyl radicals. Finally, the hydroxyl radicals destruct CDs structure and therefore cause fluorescence quenching.

Figure 8a demonstrates that the fluorescence intensity falls with the raise in H_2O_2 concentration. First, the optimum reaction condition for H_2O_2 including Fe (II) concentration and environmental pH levels is analyzed. We first measured the optimum Fe (II) addition when preparing Fe (II)-CDs from CDs. It is observed from figure 7a that the fluorescence intensity reaches its peak with the conditions of 5 mM of Fe (II), which represents the optimum concentration for the developed system. Figure 7b demonstrate the fluctuations of the Fe-CDs' fluorescence intensity with 6 distinct pH levels, which reveals an ideal pH condition of 5 for Fe (II)-CDs to have a maximum fluorescence emission. Furthermore, it can be observed that a 340 nm ultra-violet light induced the highest level of fluorescence (Figure 3c). To sum up, an optimum detection environment for H_2O_2 detection is composed with 5mM Fe (II) addition when preparing Fe (II)-CDs, a pH condition of 5, and a 340nm ultra-violet light exposure.

The detection limits as well as the linear range for H_2O_2 detecting system is also obtained. Figure 8a depicts that while the concentration of H_2O_2 stays within 0-95μM, the H_2O_2 concentrations is inversely proportional to the fluorescence intensity. Thus, within a 3 signal-

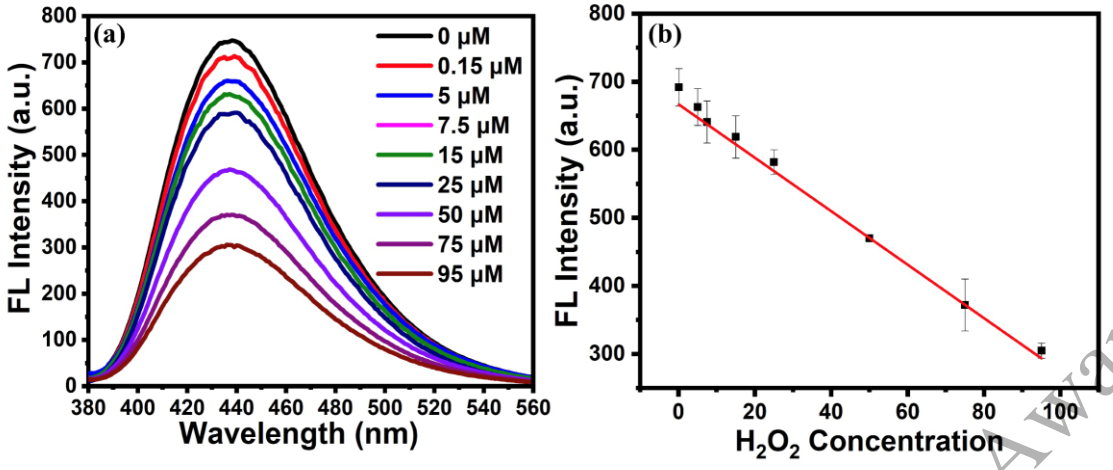

Figure. 8 The fluorescence spectrum of the H_2O_2 dependent fluorescence intensity variations in the H_2O_2 oxidation reaction (a). The data displays the linear calibration between the Fe (II)-CDs' fluorescence intensity along with the H_2O_2 addition (0-95μM) (b).

to-noise ratio, 1.00 and 0.043 μM is measured as the linear gradient and the limit of detection for this system respectively, which show a competitive accuracy with other common H_2O_2 detection methods [42-44].

The feasibility of glucose detection system is analyzed within a condition that is similar to the above mentioned one (figure 7a and 7b). It is demonstrated that Fe (II)-CDs accompanied by Glucose and GOx can cause dramatic fluorescence quenching (figure 10a).

The optimum reaction condition for glucose detection is investigated. The optimum amount of GOx addition is obtained. Figure 9a shows the glucose fluorescence intensity of Fe (II) after the addition of different amounts of GOx ranging from 0-15 U/LM. It is analyzed that a maximum fluorescence intensity is gained when 5U/ml of GOx is added. The optimum reaction time is also measured. With the addition of 5U/ml of GOx, it is observed that the fluorescence intensity is maximized after 30 min from the start of the reaction (figure 9b). In conclusion, a condition of 5U/ml of GOx addition accompanied with 30 min reaction time is the optimum condition for the developed glucose detecting system.

The linear relationship as well as the limit of detection for this glucose detecting system is therefore been measured. Figure 10b demonstrates that a decrease in terms of the Fe (II)-CDs' fluorescence intensity will be observed when an increase amount of glucose is added into the solution. The linear range of the as-developed system is measured to be in the range of 0.005-

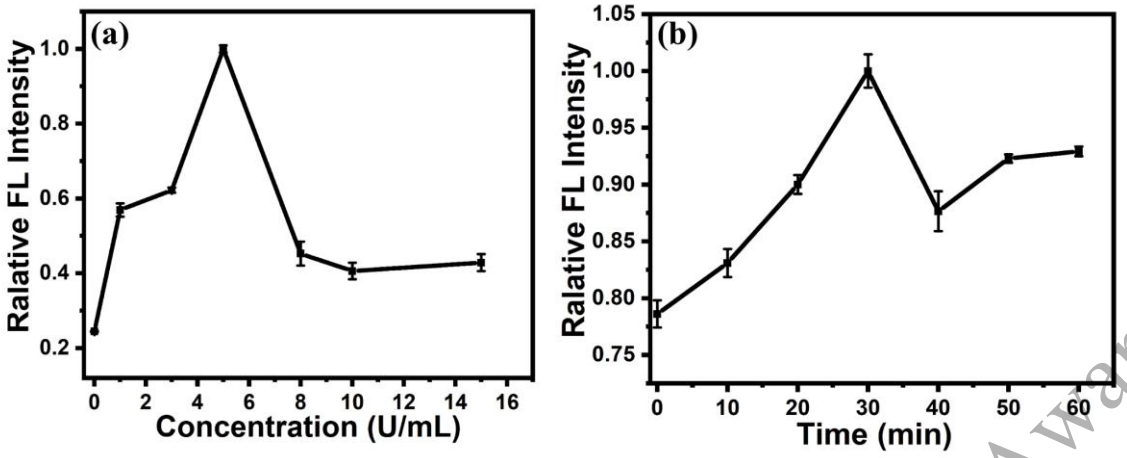

Figure. 9 A fluorescence spectrum showing the change of fluorescence intensity along with different addition of GOx into the system (a). The fluorescence spectrum illustrating the change of fluorescence intensity with time after the addition of GOx (b).

1.250 mM (R=-1.0) (figure 10c) and 1.42 μM, which is obtained under the 3 signal-to-noise ratios, is the measured value for the limit of detection.

In comparison with several reported fluorescence-utilized glucose detection methods listed (table 3), the as-prepared glucose detection system displays a wider linear range and a relatively lower limit of detection. Additionally, compare to other traditional quantum dots - for instance the traditional metal quantum dots - carbon quantum dots display high stability, low cost, environmentally friendly, great biocompatibility, water dispersibility, versatility as well as its label-free ability

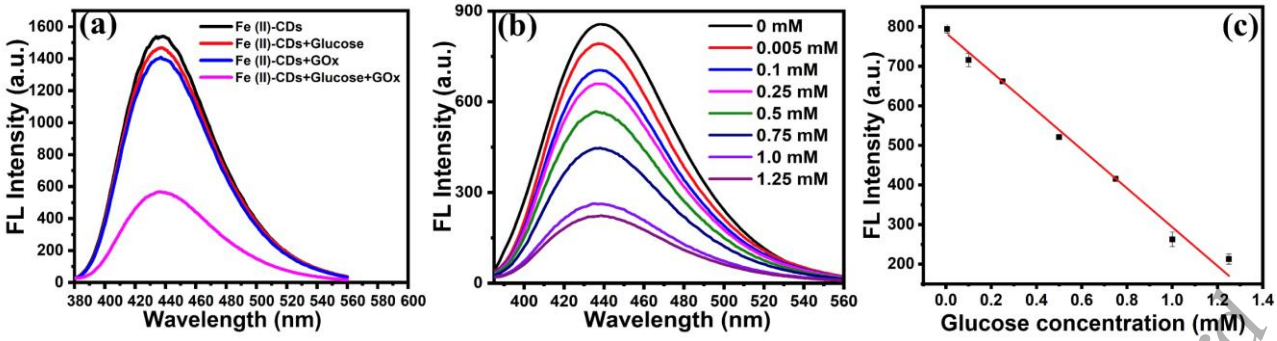

Figure. 10 The fluorescence spectrum of Fe (II)-CDs, Fe (II) CDs + Glucose, Fe (II)-CDs + GOx and Fe (II) CDs + Glucose + GOx (a). The fluorescence spectrum of the H_2O_2 dependent fluorescence intensity variations in the glucose detection system (b). The data that shows the linear calibration between the Fe (II)-CDs' fluorescence intensity and the amount of glucose addition (0-1.25 mM) (c).

Table 3. A comparison of the detection limits and linear range of different glucose detection system using fluorescence nanomaterials

Detection methods	Detection limit	Linear range	Reference
Gated mesoporous silica nanobiosensor for glucose sensing	1.5×10^5nM	1×10^5 nM-1×10^7 nM	49
Fluorescent nanostructured glucose biosensor chip utilizing glucose oxidase	5×105nM	5×105nM-1.6×105nM	50
Nanostructured fluorescence resonance energy transfer nanobiosensor for monitoring tear glucose	4×10^7nM	4×10^7nM-4×10^9nM	51
FRET quenching sensor	3×10^7 nM	3×10^7 nM-3×10^9 nM	52
Single-walled carbon nanotube nanobiosensor	2.5×10^6 nM	2.5×10^6 nM-5×10^7 nM	53
Upconverting nanomaterials-based fluorescent glucose nanobiosensor	6.4×10 nM	1×10^2 nM-5×10^3 nM	54
UCP–GO biosensor	2.5×10 nM	5.6×10^2 nM-2×10^3 nM	55
Fluorescent silver nanocluster as biosensor	1×10^4 nM	5×10^3 nM-1.7×10^5 nM	56
Ferrous Ion Immobilized Carbon Dots Fluorescent Sensing Platform for Homogeneous Glucose Detection based on Fenton Reaction	1.42×10^3 nM	5×10^3-1.25×10^6 nM	This study

property [48]. These desirable features make the as-designed glucose detection system owns more potential in biological researches.

In order to examine the as-proposed glucose detecting system's feasibility in real human serum, the selectivity of the Fe (II)-CDs (figure 11) is examined in several common substances that exist in serum, including glucose, IFN-Y, lactose, PDGF-BB, NaCl, $CaCl_2$, $MgCl_2$, thrombin and BSA [45-47], where the Fe (II)-CDs fluorescence quenching happened dramatically in the presence of glucose while it had no apparent change with other substances listed. This result shows a high selectivity of the Fe (II)-CDs in serum.

Moreover, the developed glucose detection system has been used in human serum samples (table 4). Different glucose solution at different concentrations was added to a 2.5% diluted human serum sample. The intensity of fluorescence in the solution demonstrated a decreasing trend. Furthermore, this standard recovery rate of glucose in human serum samples that are analyzed shows a fluctuation between 97.8-105.5% with an RSD value lower than 5.0%.

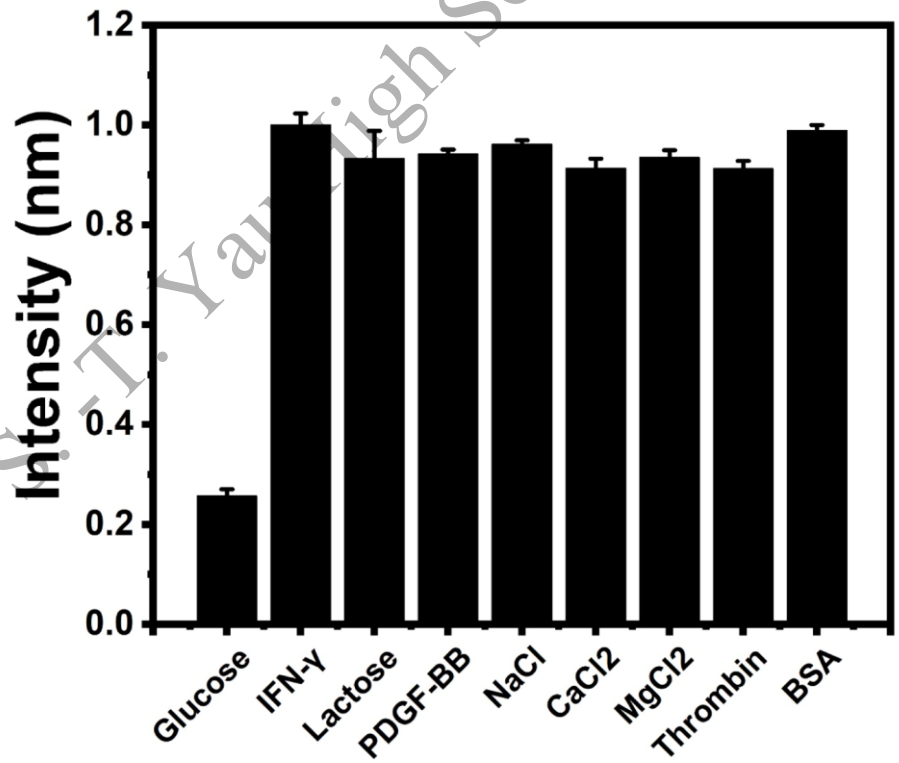

Figure. 11 A bar chart illustrates the fluorescence intensity of Fe (II)-CDs in various substances that are common in serum (glucose, IFN-Y, lactose, PDGF-BB, NaCl, CaCl2, MgCl2, Thrombin, BSA, where their concentrations are 1 μM, 2 μM, 2.5 μM, 2.5 μM, 2.5 μM, 5 μM, 5 μM are 5 μM respectively.)

Table 4. The glucose standard recovery test in human serum samples

Samples	Added (mM)	Found (mol/L)	RSD (%, n=3)	Recovery (%)
1	0	0.0038	3.1	-
2	0.005	0.0087	4.0	97.8
3	0.02	0.0249	3.6	105.5
4	0.1	0.1022	2.9	98.4
5	1.0	1.0288	3.2	102.5

4. Conclusion

In conclusion, an easy-manufacture Fe (II)-CDs complex that is low-cost, label free, environmentally friendly and has a high level of stability is developed. A serum glucose level detection methodology is then constructed utilized the Fe (II)-CDs complex. It has been demonstrated that the glucose detection system has a high level of sensitivity, selectivity and reproducibility. Possible fluorescence and quenching mechanisms were studied by ultra-violet absorption spectrum, fluorescence emission spectrum, FTIR, XPS, and zeta potential. The dominant quenching mechanism correlates to the oxidative quenching caused by the Fenton's-reaction created hydroxyl radicals. For this reason, it can be applied to H_2O_2 and hydroxyl radical detection. In light of the above-mentioned experimental results, the developed detection system owns potential in human serum glucose level detection.

references

[1] Zhao L, Wu G, Cai Z, Zhao T, Yao Q, & Chen X. Ultrasensitive non-enzymatic glucose sensing at near-neutral pH values via anodic stripping voltammetry using a glassy carbon electrode modified with Pt 3 Pd nanoparticles and reduced graphene oxide[J]. *Microchimica Acta*, 2015, 182(11-12): 2055-2060.

[2] Nathan D M. Long-term complications of diabetes mellitus[J]. *New England Journal of Medicine*, 1993, 328(23): 1676-1685.

[3] Devi R D H, Bai A, Nagarajan N. A novel hybrid approach for diagnosing diabetes mellitus using farthest first and support vector machine algorithms[J]. *Obesity Medicine*, 2020, 17: 100152.

[4] Saiti K, Macaš M, Lhotská L, Štechová K, & Pithová P. Ensemble methods in combination with compartment models for blood glucose level prediction in type 1 diabetes mellitus[J]. *Computer Methods and Programs in Biomedicine*, 2020, 196: 105628.

[5] Wang Y, Han C, Yu L, Wu J, Min Y, Tan J, Zhang P. Etching-controlled suppression of fluorescence resonance energy transfer between nitrogen-doped carbon dots and Ag nanoprisms for glucose assay and diabetes diagnosis[J]. *Spectrochimica Acta Part A: Molecular and Biomolecular Spectroscopy*, 2020: 118713.

[6] Feng X, Wang G, Li N. I, Lyu Z, Chen S, Wei L, Cui H. The association between fasting blood glucose and the risk of primary liver cancer in Chinese males: a population-based prospective study[J]. *British journal of cancer*, 2017, 117(9): 1405-1411.

[7] Cao X, Wang N, Jia S, & Shao Y. (2013). Detection of glucose based on bimetallic PtCu nanochains modified electrodes[J]. *Analytical chemistry*, 2013, 85(10): 5040-5046.

[8] Chen R, Xu W, Xiong C, Zhou X, Xiong S, Nie Z, Chang H. High-salt-tolerance matrix for facile detection of glucose in rat brain microdialysates by MALDI mass spectrometry[J]. *Analytical chemistry*, 2012, 84(1): 465-469.

[9] Freunscht P, Van Duyne R P, Schneider S. Surface-enhanced Raman spectroscopy of trans-stilbene adsorbed on platinum-or self-assembled monolayer-modified silver film over nanosphere surfaces[J]. *Chemical Physics Letters*, 1997, 281(4-6): 372-378.

[10] Xia Y, Ye J, Tan K, et al. Colorimetric visualization of glucose at the submicromole level in serum by a homogenous silver nanoprism–glucose oxidase system[J]. *Analytical chemistry*, 2013, 85(13): 6241-6247.

[11] Cao X, Wang N, Jia S, & Shao Y. (2013). Detection of glucose based on bimetallic PtCu nanochains modified electrodes[J]. *Analytical chemistry*, 2013, 85(10): 5040-5046.

[12] Lan D, Li B, Zhang Z. Chemiluminescence flow biosensor for glucose based on gold nanoparticle-enhanced activities of glucose oxidase and horseradish peroxidase[J]. *Biosensors and Bioelectronics*, 2008, 24(4): 934-938.

[13] Li J, Li Y, Shahzad S A, Chen J, Chen Y, Wang Y, Yu C. Fluorescence turn-on detection of glucose via the Ag nanoparticle mediated release of a perylene probe[J]. *Chemical Communications*, 2015, 51(29): 6354-6356

[14] Campuzano S, Yáñez-Sedeño P, Pingarrón J M. Carbon dots and graphene quantum dots in electrochemical biosensing[J]. *Nanomaterials*, 2019, 9(4): 634.

[15] Teng X, Ma C, Ge C, Yan M, Yang J, Zhang Y, Bi H. Green synthesis of nitrogen-doped carbon dots from konjac flour with "off–on" fluorescence by Fe 3+ and L-lysine for bioimaging[J]. *Journal of Materials Chemistry B*, 2014, 2(29): 4631-4639.

[16] Yang M, Liu M, Wu Z, He Y, Ge Y, Song G & Zhou J. Carbon dots co-doped with nitrogen and chlorine for "off-on" fluorometric determination of the activity of acetylcholinesterase and for quantification of organophosphate pesticides[J]. *Microchimica Acta*, 2019, 186(8): 585.

[17] Li Y, Hu Y, Zhao Y, Shi G, Deng L, Hou Y & Qu L. An electrochemical avenue to green-luminescent graphene quantum dots as potential electron-acceptors for photovoltaics[J]. *Advanced materials*, 2011, 23(6): 776-780.

[18] Song Y, Zhu S, Zhang S, Fu Y, Wang L, Zhao X, & Yang B. Investigation from chemical structure to photoluminescent mechanism: a type of carbon dots from the pyrolysis of citric acid and an amine[J]. *Journal of Materials Chemistry C*, 2015, 3(23): 5976-5984.

[19] Li L, Lu C, Li S, Liu S, Wang L, Cai W, & Zhang R. A high-yield and versatile method for the synthesis of carbon dots for bioimaging applications[J]. *Journal of Materials Chemistry B*, 2017, 5(10): 1935-1942.

[20] Yang Y, Kong W, Li H, Liu J, Yang M, Huang H, & Zhong J. Fluorescent N-doped carbon dots as in vitro and in vivo nanothermometer[J]. *ACS applied materials & interfaces*, 2015, 7(49): 27324-27330.

[21] Yang Z C, Wang M, Yong A M, Wong S Y, Zhang X H, Tan H, & Wang. J. Intrinsically fluorescent carbon dots with tunable emission derived from hydrothermal treatment of glucose in the presence of monopotassium phosphate[J]. *Chemical communications*, 2011, 47(42): 11615-11617.

[22] Nandi S, Malishev R, Kootery K P, Mirsky Y, Kolusheva S, & Jelinek R. Membrane analysis with amphiphilic carbon dots[J]. *Chemical Communications*, 2014, 50(71): 10299-10302.

[23] Shi L, Zhou G, Xiang X, Zhang Z, Jia Y, Liu P, & Li Z. Nitrogen-sulfur co-doped pH-insensitive fluorescent carbon dots for high sensitive and selective hypochlorite detection[J]. *Spectrochimica Acta Part A: Molecular and Biomolecular Spectroscopy*, 2020: 118721.

[24] Minda H, Larque E, Koletzko B, & Decsi T. Systematic review of fatty acid composition of plasma phospholipids of venous cord blood in full-term infants[J]. *European journal of nutrition*, 2002, 41(3): 125-131.

[25] Zhu S, Song Y, Zhao X, Shao J, Zhang J, & Yang B. The photoluminescence mechanism in carbon dots (graphene quantum dots, carbon nanodots, and polymer dots): current state and future perspective[J]. *Nano research*, 2015, 8(2): 355-381.

[26] Baskoutas S, Terzis A F. Size-dependent band gap of colloidal quantum dots[J]. *Journal of applied physics*, 2006, 99(1): 013708.

[27] Rolo A G, Vasilevskiy M I, Gaponik N P, et al. Confined optical vibrations in CdTe quantum dots and clusters[J]. *physica status solidi (b)*, 2002, 229(1): 433-437.

[28] Yan F, Sun Z, Zhang H, Sun X, Jiang Y, & Bai Z. The fluorescence mechanism of carbon dots, and methods for tuning their emission color: a review[J]. *Microchimica Acta*, 2019, 186(8): 583.

[29] Kasprzyk W, Świergosz T, Bednarz S, Walas K, Bashmakova N V, & Bogdał D. Luminescence phenomena of carbon dots derived from citric acid and urea–a molecular insight[J]. *Nanoscale*, 2018, 10(29): 13889-13894.

[30] Mintz K J, Zhou Y, Leblanc R M. Recent development of carbon quantum dots regarding their optical properties, photoluminescence mechanism, and core structure[J]. *Nanoscale*, 2019, 11(11): 4634-4652.

[31] Wang R, Wang X, Sun Y. One-step synthesis of self-doped carbon dots with highly photoluminescence as multifunctional biosensors for detection of iron ions and pH[J]. *Sensors and Actuators B: Chemical*, 2017, 241: 73-79.

[32] Lakowicz J R. Plasmonics in biology and plasmon-controlled fluorescence[J]. *Plasmonics*, 2006, 1(1): 5-33.

[33] Zu F, Yan F, Bai Z, Xu J, Wang Y, Huang Y, & Zhou X. The quenching of the fluorescence of carbon dots: a review on mechanisms and applications[J]. *Microchimica Acta*, 2017, 184(7): 1899-1914.

[34] Zhang Y, Wang L, Zhang H, Liu Y, Wang H, Kang Z, & Lee S. Graphitic carbon quantum dots as a fluorescent sensing platform for highly efficient detection of Fe 3+ ions[J]. *RSC advances*, 2013, 3(11): 3733-3738.

[35] Wang R, Wang X, Sun Y. One-step synthesis of self-doped carbon dots with highly photoluminescence as multifunctional biosensors for detection of iron ions and pH[J]. *Sensors and Actuators B: Chemical*, 2017, 241: 73-79.

[36] Liu M L, Chen B B, Li C M, & Huang C Z. Carbon dots prepared for fluorescence and chemiluminescence sensing[J]. *Science China Chemistry*, 2019: 1-14.

[37] Chipman D M. Absorption spectrum of OH radical in water[J]. *The Journal of Physical Chemistry A*, 2008, 112(51): 13372-13381.

[38] Molina L T, Schinke S D, Molina M J. Ultraviolet absorption spectrum of hydrogen peroxide vapor[J]. *Geophysical Research Letters*, *1977*, 4(12): 580-582.

[39] Lee H J, Jana J, Chung J. S, & Hur S H. Uncovering the actual inner-filter effect between highly efficient carbon dots and nitroaromatics[J]. *Spectrochimica Acta Part A: Molecular and Biomolecular Spectroscopy*, 2020: 118342.

[40] Song Y, Zhu S, Xiang S, Zhao X, Zhang J, Zhang H, & Yang B. Investigation into the fluorescence quenching behaviors and applications of carbon dots[J]. *Nanoscale*, 2014, 6(9): 4676-4682.

[41] Pan X, Zhang Y, Sun X, Pan W, & Wang J. A green emissive carbon-dot-based sensor with diverse responsive manners for multi-mode sensing[J]. *Analyst*, 2018, 143(23): 5812-5821.

[42] Xu J, Zhang Y, Yu H, Gao X, & Shao S. Mitochondria-targeted fluorescent probe for imaging hydrogen peroxide in living cells[J]. *Analytical chemistry*, 2016, 88(2): 1455-1461.

[43] Chakraborty D, Sarkar S, Das P K. Blood dots: hemoglobin-derived carbon dots as hydrogen peroxide sensors and pro-drug activators[J]. *ACS Sustainable Chemistry & Engineering*, 2018, 6(4): 4661-4670.

[44] Liu X, He L, Yang L, Geng Y, Yang L, & Song X. Iminocoumarin-based fluorescence probe for intracellular H2O2 detection with a red emission and a large Stokes shift[J]. *Sensors and Actuators B: Chemical*, 2018, 259: 803-808.

[45] PSI Structural Biology Knowledgebase. (n.d.). Retrieved August 06, 2020, from http://sbkb.org/fs/serum-albumins-and-allergies

[46] Razaghi A, Owens L, Heimann K. Review of the recombinant human interferon. gamma as an immunotherapeutic: Impacts of production platforms and glycosylation[J]. *Journal of biotechnology*, 2016, 240: 48-60.

[47] Di Cera E. Thrombin[J]. *Molecular aspects of medicine*, 2008, 29(4): 203-254.

[48] Dutta A K, Das S, Samanta S, Samanta P K, Adhikary B, & Biswas P. CuS nanoparticles as a mimic peroxidase for colorimetric estimation of human blood glucose level[J]. *Talanta*, 2013, 107: 361-367.

[49] Aznar E, Villalonga R, Giménez C, Sancenón F, Marcos M D, Martínez-Máñez. R, & Amorós P. Glucose-triggered release using enzyme-gated mesoporous silica nanoparticles[J]. *Chemical communications*, 2013, 49(57): 6391-6393.

[50] Li X, Zhou Y, Zheng Z, Yue X, Dai Z, Liu S, & Tang Z. Glucose biosensor based on nanocomposite films of CdTe quantum dots and glucose oxidase[J]. *Langmuir*, 2009, 25(11): 6580-6586.

[51] Zhang J, Wang X, Chen L, Li J, & Luzak K. Harnessing a nanostructured fluorescence energy transfer sensor for quick detection of extremely small amounts of glucose[J]. 2013.

[52] Chen L, Tse W H, Chen Y, McDonald, M W, Melling J, & Zhang J. Nanostructured biosensor for detecting glucose in tear by applying fluorescence resonance energy transfer quenching mechanism[J]. *Biosensors and Bioelectronics*, 2017, 91: 393-399.

[53] Yoon H, Ahn J H, Barone P W, Yum K, Sharma R, Boghossian A A, & Strano M. S. Periplasmic Binding Proteins as Optical Modulators of Single-Walled Carbon Nanotube Fluorescence: Amplifying a Nanoscale Actuator[J]. *Angewandte Chemie*, 2011, 123(8): 1868-1871.

[54] Liu J, Lu L, Li A, Tang J, Wang S, Xu S, & Wang L. Simultaneous detection of hydrogen peroxide and glucose in human serum with upconversion luminescence[J]. *Biosensors and Bioelectronics*, 2015, 68: 204-209.

[55] Zhang C, Yuan Y, Zhang S, Wang Y, & Liu Z. Biosensing platform based on fluorescence resonance energy transfer from upconverting nanocrystals to graphene oxide[J]. *Angewandte Chemie International Edition*, 2011, 50(30): 6851-6854.

[56] Dong J X, Gao Z F, Zhang Y, Li B L, Zhang W, Lei J L, & Luo H Q. The pH-switchable agglomeration and dispersion behavior of fluorescent Ag nanoclusters and its applications in urea and glucose biosensing[J]. *NPG Asia Materials*, 2016, 8(12): e335-e335.

Acknowledgement

We are grateful to Mr. Shah for the insight that inspired us in terms of essay writing and topic development. With his guidance, we are able to gain more inspirations on topic researching and therefore strengthens our essay's logic. In light of the above-mentioned reasons, this study cannot be done with this standard without the help of Mr. Shah.